Unusual spiral wave tip trajectories in a parametrically forced nonequilibrium system

Jysoo Lee,* Jinha Kim, Goen-hee Yi, and Kyoung J. Lee†
National Creative Research Initiative Center for Neurodynamics and Department of Physics, Korea University, Seoul 136-701, Korea
(Received 25 September 2001; published 28 March 2002)

The effect of parametric modulations on spiral waves that form in a thin layer of liquid crystal under rotating magnetic field is studied in laboratory experiments and numerical simulations. Parametric forcings that are sinusoidal in time make a simply rotating spiral tip to meander, rendering a compound tip trajectory that is composed of a main circular orbit and a satellite orbit with an unusual crescent shape. No evidence of frequency locking is found. The underlying mechanism for the unusual shape of the satellite orbit is elucidated, and the dependence of the rotation frequency of the main circular orbit $\tilde{f}_o$ on the perturbation parameters are discussed.

DOI: 10.1103/PhysRevE.65.046207 PACS number(s): 47.54.+r, 05.45.Xt, 61.30.Jf, 42.60.Fc

I. INTRODUCTION

Spiral waves are ubiquitous in nature and perhaps the best known nonequilibrium structure investigated so far. Various issues have been raised and studied regarding them during the last few decades [1–9]. Nonetheless, spiral waves in nonequilibrium systems are still an important research topic. Among others, one of the up-to-date issues is to understand the effect of extrinsic stimuli on the dynamics of spiral waves. This issue is not only a very interesting theoretical problem [10–13] but also has a good potential application in cardiology [7,14,15]. There are only a few past studies on this topic.

For example, Steinbock *et al.* investigated a light-sensitive Belousov-Zhabotinsky (BZ) reaction-diffusion system with external light perturbations, in particular, in an excitable regime [16]. Their study was mainly focused on the case that the unperturbed spiral executes a meandering rotation (i.e., the spiral core executes a compound orbit formed by two circular motions combined). The external periodic perturbation that was homogeneous in space while sinusoidally varying in time had resulted in a variety of complex tip trajectories that were either closed (i.e., periodic with a frequency locking) or opened (i.e., quasiperiodic without a frequency locking) depending on the parameter values. Parametrically modulated spirals in excitable system were also investigated in model systems. Among others, one interesting conclusion is that rigidly rotating spirals can only have a resonant drift upon small amplitude parametric modulations [17,18].

More recently, Swinney and co-workers investigated the same issue using a BZ experimental system but in an oscillatory regime [19,20]. Their results were dramatically different from those of Steinbock *et al.* [16]. Unlike the case of excitable spirals, the spirals in oscillatory regime were all unstable to the applied light modulations. In other words, the initial spirals all disappeared with the perturbation. Instead, various resonant patterns—stationary fronts, standing waves of labyrinth, and more complex structures—were emerged. Recently, Vanag and co-workers had done a more detailed investigation in a similar oscillatory regime and found yet another interesting localized structures [21,22]. These experimental results and the recent numerical simulation studies [23,24], all together suggest that spiral forming systems under external forcing are indeed a very rich dynamical system.

Here, we note that all previous investigations on externally forced spiral waves have been limited to the ones associated with BZ reaction-diffusion systems. Thus, it is not known or at least unclear what would be the outcome of parametric modulation given to spiral waves in different systems. This motivated us to investigate the dynamics of periodically modulated spiral waves forming in a thin layer of nematic liquid crystal that rotates under uniform magnetic fields [25–27]. The spiral wave in the liquid crystal system is a domain wall, while the ones in reaction-diffusion systems originate from the local nonlinear kinetics that is either excitable or oscillatory.

We find that forced liquid crystal systems also produce meandering spiral waves whose tip trajectory is very analogous to the compound orbits observed in Refs. [16,28–30]. The compound trajectories in the forced liquid crystal system, however, distinguish themselves from a typical epycloid orbit for the fact that their secondary orbits are not a simple circle but a crescent-shaped loop. Besides, no case of frequency-locked compound orbit is realized within our extensive parameter search. Numerical simulations on a modified time dependent Ginzburg-Landau equation (TDGL) modeling the forced liquid crystal system are also carried out, and the results are quite consistent with the experimental results.

II. EXPERIMENT

A. Setup

Our experimental system is modeled after the one in Ref. [27]. The spirals form in a thin Hele-Shaw cell filled with nematic liquid crystal *N*-(4-methoxybenzylidene)-4-butylaniline (Sigma-Aldrich Chemical), rotating under uniform magnetic field (see Fig. 1). The gap between two glass

*Current address: Supercomputing Center, Korea Institute of Science and Technology Information, P.O. Box 122, Yusong, Daejon 305-806, Korea.

†Author to whom correspondence should be addressed. Electronic adress: kyoung@nld.korea.ac.kr

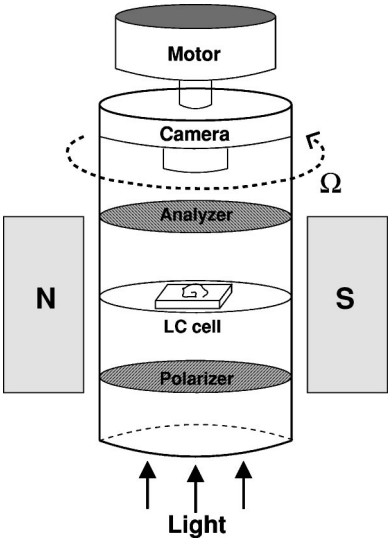

FIG. 1. Experimental setup for studying parametrically forced spiral waves. The system is composed of a Hele-Shaw cell filled with homeotropically aligned liquid crystal layer (LC cell), an electromagnet, and optics for imaging. The whole assembly is attached to a step motor. Domain walls appear black through the analyzer. The setup is temperature regulated at $(28.0\pm0.1)\,^{\circ}$C.

plates is 75 μm thick, and the lateral dimension of the cell is 21×18 mm^2. The inner surfaces of the glass plates are coated with *n*-Hexadecyltrimethylammonium bromide (Kanto Chemical) to align the molecules normal to the surfaces (i.e., homeotropic alignment). Uniform magnetic field is applied in a direction transverse to the director field (i.e., normal to the *z* axis) with an electromagnet (ANAC, Precision Electromagnet) whose iron core is 7.5 in. in diameter. The distance between two iron cores is 4 in. Images of director field are visualized with a halogen light source and two cross polarizers, acquired through a (1/3)-in. charge coupled device camera (WAT-902A, Watec) equipped with a micro video zoom objective lens (Tzvoa, Titan Tool Supply), and digitized by a frame grabber (Meteor, Metrox).

The polarizer, the Hele-Shaw cell, the analyzer, and the video camera assembly, all are mounted on a single acrylic tube that is again coupled to a computer-controlled step motor as shown in Fig. 1. A 12-bit digital signal is generated from an home-made synthesizer board with a programmable peripheral interface device (82C55A, Intel) and converted to an analog signal with a digital-to-analog converter (DAC7625, Burr Brown). Subsequently, the analog signal is sent to a voltage/frequency converter (LM331N, National Semiconductor) whose output is fed to a motor driver. The motor driver itself consists of a step motor controller (L297, SGS-Thomson) and an unipolar step motor controller (SLA7024, Allegro). The rotation frequency of the step motor can be easily modulated by changing the digital pulse signal from the synthesizer board. The step resolution of the motor with a worm gear of 1:15 reduction ratio is $0.12\,^{\circ}$. Unless mentioned otherwise, spiral images are acquired at every $90\,^{\circ}$ rotation (i.e., four frames per a complete rotation) to keep the overall brightness of the image to be constant.

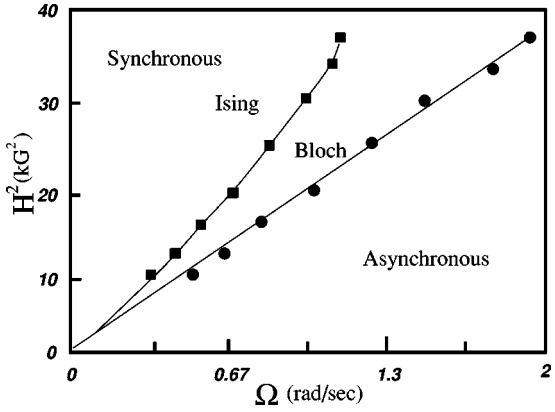

FIG. 2. Phase diagram showing synchronous-asynchronous transition (line with filled circle) and Ising-Bloch transition (line with filled square). H is the magnetic field and Ω is the instantaneous angular velocity of the sample about the z axis.

B. Constant rotation velocity

When the magnetic field is applied to the homeotropically aligned sample, two physical factors compete each other in the system: (1) the molecules tend to align along the applied magnetic field since the diamagnetic anisotropy of the liquid crystal is positive, while (2) the elastic deformation force tries to keep the molecules parallel to the z axis. As the applied field strength increases beyond a critical value, the director field suddenly becomes parallel (or antiparallel) to the applied field—a phenomenon known as the Frederiks transition [31]. Above the transition, there exist two equivalent homogeneous states whose director fields are either parallel or antiparallel to the applied field.

The Hele-Shaw cell in our experimental system rotates as shown in Fig. 1. In this case, the angular frequency Ω_o of the rotation as well as the applied field strength H becomes a relevant parameter governing the dynamics of the director field. According to the values of these two parameters, the director fields can be either ''synchronous'' or ''asynchronous'' to the applied magnetic field (see Fig. 2) [32]. In the synchronous regime, the parallel and the antiparallel director field states both are stable, thus they can coexist forming domains that are bounded by domain walls. The walls themselves can be either Ising- or Bloch-type depending on the parameter values [33]. An Ising wall is static, while a Bloch wall moves with a constant velocity.

Domain walls in a form of rotating spiral can arise in the Bloch wall regime as shown in Fig. 3. They either arise spontaneously from the inhomogeneities of the system or can be induced by some finite amplitude perturbations. For example, the particular example shown in Fig. 3 is generated by quenching parameter values rapidly near the Ising-Bloch transition as described in [25–27,34]. The spiraling domain wall rotates rigidly about its center, thus the two spiral tips [35] both trace a circle as shown in Fig. 3. The domain walls in a form of spiral wave rotate rigidly as long as they are not perturbed externally. The radius of the circular tip trajectory decreases monotonically as a function of Ω.

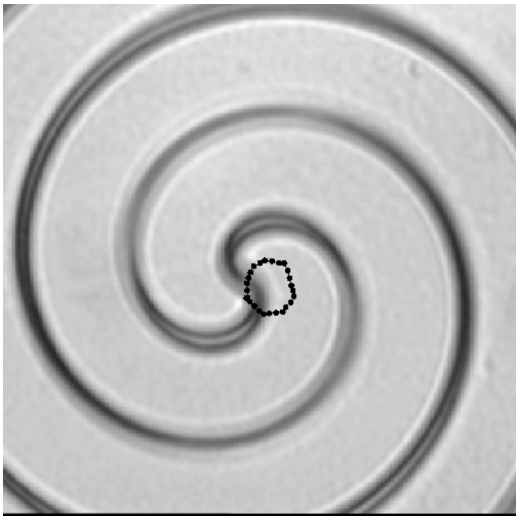

FIG. 3. A rigidly rotating spiral wave in the absence of parametric forcing and its circular tip trajectory (for 24.4 sec duration) superimposed. The viewing area is 1.2 mm$\times$1.2 mm. $\Omega_o = 1.68$ rad/sec and $H = 5.00$ kG. The spiral rotation frequency f_o is measured to be 4.41×10^{-2} sec^{-1}.

C. Modulated rotation velocity

The effect of parametric forcing is studied by making the rotation frequency Ω time dependent such that $\Omega(t) = \Omega_o + A\sin(2\pi ft)$. Perturbation experiments are carried out for three different sets of (Ω_o, H) values in Bloch regime. For each set of (Ω_o, H), five different values of f and three different values of A are studied. Sequential images of perturbed spirals are acquired, and their tip locations are identified. Typically, 1000 successive frames are captured for each run, which roughly corresponds to 40 spiral rotations. The maximum number of images that can be acquired at a time is limited by the presence of wave trains that move fast into the system from the cell boundary or from pacemakers. They always entrain spiral waves.

The spirals in the forced liquid crystal system all have survived the given parametric modulations that we introduced. However, the modulation makes the initially circular tip trajectories wobble as shown in Figs. 4(a)–4(c). The perturbed tip typically follows a compound orbit that is very analogous to the hypercloid (or epycloid) orbits observed in the excitable BZ system of Ref. [16]. Unlike the perturbed BZ system, however, no frequency-locking phenomenon is observed in our system, and the shape of the observed satellite orbit is in general not a simple circle but resembles a crescent. The shape of the satellite orbit gradually transforms from a circle to a crescent as the modulation frequency is lowered [see Fig. 4(d)]. A similar gradual change from a circule to a crescent orbit is also observed when A is increased while f is fixed. The rotation frequency of the primary circular orbit $\tilde{f}_o$ depends crucially on the values of A and f, while the rotation frequency of the satellite orbit is always the same as the imposed modulation frequency f. Essentially, the same behaviors are observed for all three different values of (Ω_o, H), or with a different sample.

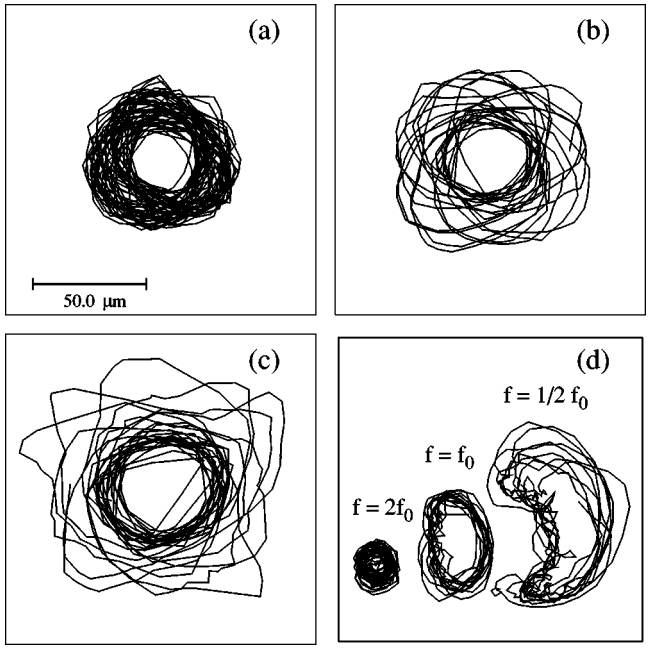

FIG. 4. Spiral tip trajectories under parametric modulations (experiment). Each trajectories is plotted for a duration of about 10 min. The modulation frequency f decreases from (a) $2f_o$, (b) f_o to (c) $f_o/2$. Here, $f_o(=4.41\times10^{-2}\ \text{sec}^{-1})$ is the rotation frequency of the unperturbed spiral. All other parameters are fixed: $A = 0.29$ rad/sec, $\Omega_o = 1.68$ rad/sec, and $H = 5.00$ kG, respectively. (d) Satellite orbits associated with the trajectories shown in (a)–(c). The satellite orbits are isolated from the compound orbits by rotating every points along the trajectory by $-2\pi\tilde{f}_o t$ around the center, where $\tilde{f}_o$ the detuned angular frequency of the primary circular orbit. The three satellite orbits shown in (d) do not share a common origin of the coordinate system—they are scaled but displaced in a way that they do not overlap each other.

III. NUMERICAL SIMULATION

A. Simulation method

In the present experimental setup, it is very difficult to quantify the modulated tip trajectories for a wide range of parameter values. Obtaining a sequence of more than a couple of thousand images is not feasible due to the pacemaker waves that entrain spiral waves. Therefore, we have compared and complemented the experimental results with numerical simulations on a model system.

When the deviation of the director field from z axis is small, its time evolution in the synchronous regime can be described by a forced time dependent Ginzburg-Landau equation [26,36]. In a dimensionless form, the equation is

$$\partial_t A = (1 - i\omega)A + \gamma\bar{A} + \nabla^2 A - |A|A, \tag{1}$$

where ω and γ are real dimensionless parameters. The complex amplitude A is $n_x + in_y$, where $n_x(n_y)$ is the $x(y)$ component of the director field.

The TDGL equation is integrated numerically with an alternating direction implicit method, which is unconditionally stable [37]. The method is of second order both in space and time. Typical value for the time step and spatial resolution is

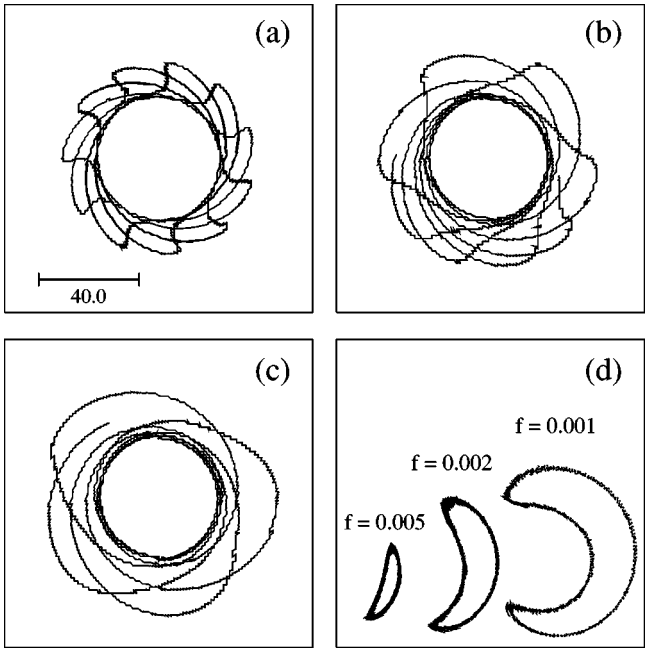

FIG. 5. Spiral tip trajectories under parametric modulations (numerical simulation). Each trajectories is plotted for a duration of 10^4 units. The modulation frequency f decreases from (a) 0.005, (b) 0.002, to (c) 0.001. All other parameters are fixed: $A=0.04$, $\omega_o=0.1$, and $\gamma=0.2$, respectively. Here, $f_o=2.09\times10^{-3}$. (d) Satellite orbits associated with the trajectories shown in (a)–(c). As in Fig. 4(d), the satellite orbits in (d) are scaled but do not share a common origin of the coordinate system.

0.025 and 0.5, respectively. The Ising-Bloch transition boundary as determined by our numerical simulations agrees well with that of the theory [26,33] and the current experiment (Fig. 2). The velocity of the Bloch wall is measured for several different values of ω and γ and found to be consistent with the existing theory as well, especially near the Ising-Bloch transition [26,33].

Rotating spiral waves of the model system are constructed as follows. The parameters ω and γ are adjusted to bring the system into a Bloch regime, and two straight Bloch walls of opposite chirality are seeded as a finite amplitude perturbation. These Bloch walls then wind around the immobile singular point to form a rotating spiral wall [25–27]. Systems with a 200×200 mesh are mainly used. Systems with a 500×500 mesh or a 1000×100 mesh are also studied to confirm that their results are not different from the ones obtained in the smaller 200×200 system.

B. Shape of satellite orbit

Effects of parametric modulations of the type $\omega(t)=\omega_o+A\sin(2\pi ft)$ are investigated with a fixed value of γ. In the absence of the parametric modulation, the tip trajectory is simply a circle. When the modulation is turned on, however, the tip trajectory starts to deviate from an initial circle and meander. In Fig. 5, tip trajectories for several different values of f are shown with A and ω_o fixed. The degree of meandering (i.e., amplitude of the deviation) gradually increases as f decreases. Such phenomenon is observed for every nonzero values of A. The other parameter γ is modulated as well in a similar fashion, but we do not find any qualitative difference.

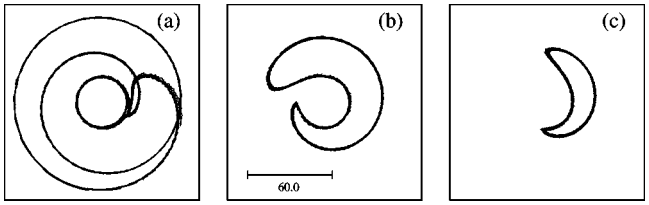

FIG. 6. Satellite orbits for different values of f: (a) $f=0.001$, (b) 0.0025, and (c) 0.005. $A=0.1$ and other parameters are the same as in Fig. 5.

As in the experiment, the satellite orbit can be isolated from a meandering trajectory by rotating every points by $-2\pi\tilde{f}_o t$ around the immobile singular point. The satellite orbits associated with the meandering trajectories of Figs. 5(a)–5(c) are thus extracted and shown in Fig. 5(d). The shape of satellite orbit gradually changes from a circle to a crescent as in the experiment. During this shape change, however, its rotation frequency stays the same as the given modulation frequency f. As far as we have explored, the meandering tip trajectories seem to be always quasiperiodic. In other words, there is no evidence of a frequency locking between the two involved frequencies $\tilde{f}_o$ and f. All these findings are very consistent with the experimental observations.

One can give a heuristic explanation for the origin of the unusual shape of the observed satellite orbits. If the modulation frequency f is quite small compared to the mean rotation frequency f_o of the primary circular motion, ω would vary from its minimum (ω_o-A) to its maximum (ω_o+A) in a quasistatic fashion. The radius of the initial circular tip trajectory would vary accordingly. One can view the perturbed trajectory as a circular orbit being acquired a satellite orbit whose radius varies in a quasi-static fashion from a maximum to a minimum value. For example, the innermost (outermost) circle in Fig. 6(a) corresponds to the value of $\omega(t)$ being close to its maximum (minimum). When f becomes large, however, the system becomes no longer quasistatic—the tip barely completes the inner (or outer) circle before moving on to the outer (or inner) circle [see Figs. 6(b) and 6(c)]. Thus, a crescent-shaped satellite orbit is formed.

C. Parameter dependence of $\tilde{f}_o$

In order to understand the dependence of $\tilde{f}_o$ on the amplitude A and the frequency f of the modulation, one can consider the movement of an linear Bloch wall. Near an Ising-Bloch transition, the velocity of a linear Bloch wall is proportional to ω [26,33]. When the parameter ω is modulated, the time averaged propagation velocity $\bar{c}$ of the wall can be shown to be

$$\bar{c}\simeq c_o+B(f)A^2 \tag{2}$$

for small A [38]. Here c_o is the velocity of the wall in the absence of modulation, and $B(f)$ is some function of f. As

the period of the modulation $1/f$ becomes smaller than the relaxation time τ of the director field, the deviation of $\bar{c}$ from c_o must get smaller. The simplest form of $B(f)$ consistent with this expectation is an exponentially decaying function of f with a decay constant of an order τ. Note that the spirals are nothing but a Bloch wall. Therefore, it is quite reasonable to assume that the rotation frequency of spirals is linearly related to $\bar{c}$. Under these assumptions,

$$\tilde{f}_o(A,f) \simeq f_o + C(f)A^2, \tag{3}$$

where $C(f)$ is an exponential function of f, which is proportional to $B(f)$. To test the validity of Eq. (3), $\tilde{f}_o(A,f)$ for 100 different combinations of A and f are measured with $\omega_o = 0.1$ and $\gamma = 0.2$. The parameter A ranges from 0.01 to 0.1, while f ranges from 0.001 to 0.01. The measured values of $\tilde{f}_o(A,f)$ agree well with the Eq. (3) for small A as shown in Fig. 7. The function is clearly quadratic in A. Moreover, the coefficient $C(f)$ can be fitted quite well with an exponential function of f. Although Eq. (3) is derived for the case that only ω is being modulated, measurements of $\tilde{f}_o(A,f)$ for the other types of modulations (both A and ω) show that the equation remains valid for even these cases.

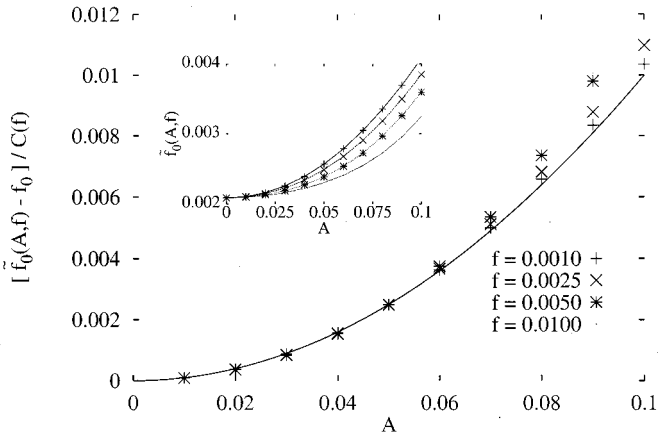

FIG. 7. The detuning of the main orbit. The rotation frequency of the main orbit $\tilde{f}_o$ is plotted as a function of A for several different values of f. Here, $\omega_o(=0.1)$ and $\gamma(=0.2)$ are constants. Shown in the inset are measured $\tilde{f}_o$ for several values of A and f. In the main figure, the data is plotted in a way to check the validity of Eq. (3). $C(f)$ is obtained by an exponential fit as discussed in the text.

IV. CONCLUSION

The effect of parametric modulations on spiral waves that form in a liquid crystal system is studied in experiments and numerical simulations. We find that the perturbed spiral tip trajectories form quasiperiodic orbits that are consisted of a circular main orbit with frequency $\tilde{f}_o(A,f)$ and a crescent shaped satellite orbit with f. Unlike the case of similar experiments conducted earlier with BZ reaction-diffusion systems [16], the perturbed spirals in our liquid crystal system show no evidence of frequency-locking. In any event, the perturbed spiral tip trajectories in our system do not become a resonant drift that is generic of modulated excitable systems [17,18]. The origin of the unusual shapes of satellite orbits and the functional form of $\tilde{f}_o$ are discussed with numerical simulations on a generic model system.

ACKNOWLEDGMENT

This work was supported by Creative Research Initiatives of the Korean Ministry of Science and Technology.

[1] *Waves and Patterns in Chemical and Biological Media*, edited by H. L. Swinney and V. I. Krinsky (MIT, North-Holland, 1992).
[2] K. J. Lee, W. D. McCormick, J. E. Pearson, and H. L. Swinney, Nature (London) **369**, 215 (1994).
[3] *Chemical Waves and Patterns*, edited by R. Kapral and K. Showalter (Kluwer, Dordrecht, 1995).
[4] K. J. Lee, E. C. Cox, and R. E. Goldstein, Phys. Rev. Lett. **76**, 1174 (1996); E. Pálsson, K. J. Lee, R. E. Goldstein, J. Franke, R. H. Kessin, and E. C. Cox, Proc. Natl. Acad. Sci. U.S.A. **94**, 13 719 (1997), and references therein.
[5] J. Lechleiter, S. Girard, D. Clapham, and E. Peralta, Nature (London) **350**, 505 (1991); L. Rensing, *Oscillations and Morphogenesis* (Marcel Dekker, New York, 1993).
[6] J. M. Davidenko, A. V. Pertsov, R. Salomonsz, W. Baxter, and J. Jalife, Nature (London) **355**, 349 (1992).
[7] L. Glass, Phys. Today **45**, 40 (1996).
[8] L. Goryachev and R. Kapral, Phys. Rev. Lett. **76**, 1619 (1996); L. Goryachev, H. Chaté, and R. Kapral, *ibid.* **80**, 873 (1998); **83**, 1878 (1999).
[9] J.-S. Park and K. J. Lee, Phys. Rev. Lett. **83**, 5393 (1999).
[10] P. Coullet and K. Emilsson, Physica D **61**, 119 (1992).
[11] D. Walgraef, *Spatio-Temporal Pattern Formation* (Springer, New York, 1997).
[12] C. Elphick, A. Hagberg, and E. Meron, Phys. Rev. Lett. **80**, 5007 (1998).
[13] H.-K. Park, Phys. Rev. Lett. **86**, 1130 (2001).
[14] *Computational Biology of the Heart*, edited by A. V. Panfilov and A. V. Holden (Wiley, Chichester, 1997).
[15] M. E. Josephson, *Clinical Cardiac Electrophysiology: Techniques and Interpretation* (Lea & Febiger, Philadelphia, 1993).
[16] O. Steinbock, V. Zykov, and S. C. Müller, Nature (London) **366**, 322 (1993).
[17] A. Mikhailov, V. Davydov, and V. Zykov, Physica D **70**, 1 (1994).
[18] R. Mantel and D. Barkley, Phys. Rev. E **54**, 4791 (1996).
[19] V. Petrov, Q. Ouyang, and H. L. Swinney, Nature (London) **388**, 655 (1997).
[20] A. Lin, M. Bertram, K. Martinez, and H. L. Swinney, Phys. Rev. Lett. **84**, 4240 (2000).

[21] V. Vanag, L. Yang, M. Dolnik, A. Zhabotinsky, and I. Epstein, Nature (London) **406**, 389 (2000).
[22] V. Vanag, A. Zhabotinsky, and I. Epstein, Phys. Rev. Lett. **86**, 552 (2001).
[23] K. J. Lee, Phys. Rev. Lett. **79**, 2907 (1997).
[24] S.-M. Hwang, W. G. Choe, and K. J. Lee, Phys. Rev. E **62**, 4799 (2000).
[25] K. B. Migler and R. B. Meyer, Physica D **71**, 412 (1994).
[26] T. Frisch, S. Rica, P. Coullet, and J. M. Gilli, Phys. Rev. Lett. **72**, 1471 (1994).
[27] S. Nasuno, N. Yoshimo, and S. Kai, Phys. Rev. E **51**, 1598 (1995).
[28] D. Barkley, Phys. Rev. Lett. **72**, 164 (1994).
[29] G. Li, Q. Ouyang, V. Petrov, and H. L. Swinney, Phys. Rev. Lett. **77**, 2105 (1996).
[30] L. Q. Zou and Q. Ouyang, Phys. Rev. Lett. **85**, 1650 (2000).
[31] P. de Gennes and J. Prost, *The Physics of Liquid Crystals* (Oxford University Press, Oxford, 1993).
[32] Similar phase diagram was reported earlier, K. B. Migler and R. B. Meyer, Phys. Rev. Lett. **66**, 1485 (1991).
[33] P. Coullet, J. Lega, B. Houchmanzadeh, and J. Lajzerowicz, Phys. Rev. Lett. **65**, 1352 (1990).
[34] J. M. Gilli, M. Morabito, and T. Frish, J. Phys. II **4**, 319 (1994).
[35] Spiral tips are defined as follows. At the singularity (i.e., center of the spiral), a line that is tangent to the wall is drawn. Similarly, tangential vectors are determined at every points along the wall. The nearest spatial point from the center, whose tangent vector is normal to the tangent line at the singularity, is defined as the tip.
[36] T. Frisch, Physica D **84**, 601 (1995).
[37] C. A. J. Fletcher, *Computational Techniques for Fluid Dynamics* (Springer, New York, 1991).
[38] J. Lee (unpublished).